

Rational Design of a Functional Metalloenzyme: Introduction of a Site for Manganese Binding and Oxidation into a Heme Peroxidase[†]

Sheri K. Wilcox, Christopher D. Putnam, Mallika Sastry, John Blankenship, Walter J. Chazin, Duncan E. McRee, and David B. Goodin*

Department of Molecular Biology, MB8, The Scripps Research Institute, 10550 North Torrey Pines Road, La Jolla, California 92037

Received June 24, 1998; Revised Manuscript Received September 22, 1998

ABSTRACT: The design of a series of functionally active models for manganese peroxidase (MnP) is described. Artificial metal binding sites were created near the heme of cytochrome *c* peroxidase (CCP) such that one of the heme propionates could serve as a metal ligand. At least two of these designs, MP6.1 and MP6.8, bind Mn²⁺ with $K_d \cong 0.2$ mM, react with H₂O₂ to form stable ferryl heme species, and catalyze the steady-state oxidation of Mn²⁺ at enhanced rates relative to WT CCP. The kinetic parameters for this activity vary considerably in the presence of various dicarboxylic acid chelators, suggesting that the similar features displayed by native MnP are largely intrinsic to the manganese oxidation reaction rather than due to a specific interaction between the chelator and enzyme. Analysis of pre-steady-state data shows that electron transfer from Mn²⁺ to both the Trp-191 radical and the ferryl heme center of compound ES is enhanced by the metal site mutations, with transfer to the ferryl center showing the greatest stimulation. These properties are perplexingly similar to those reported for an alternate model for this site (*I*), despite rather distinct features of the two designs. Finally, we have determined the crystal structure at 1.9 Å of one of our designs, MP6.8, in the presence of MnSO₄. A weakly occupied metal at the designed site appears to coordinate two of the proposed ligands, Asp-45 and the heme 7-propionate. Paramagnetic nuclear magnetic resonance spectra also suggest that Mn²⁺ is interacting with the heme 7-propionate in MP6.8. The structure provides a basis for understanding the similar results of Yeung et al. (*I*), and suggests improvements for future designs.

With the developing interest in rational design of artificial metal sites into protein structures, it has become feasible to think of creating functional enzymes and biosensors containing artificial redox active metal centers. Several studies have demonstrated the successful introduction of metal binding sites into proteins (2–9), and recently an iron binding site introduced into thioredoxin has been shown to possess weak catalytic activity as a superoxide dismutase (*10*). While the reactions catalyzed by such artificial metalloenzymes are admittedly simple as yet, these structures will provide a departure point for fine-tuning the activities and specificities of these centers. This report describes an elaboration on this approach in which we have used a protein containing an existing redox active heme cofactor as a scaffold into which several variant binding sites for a second metal ion “substrate” are introduced.

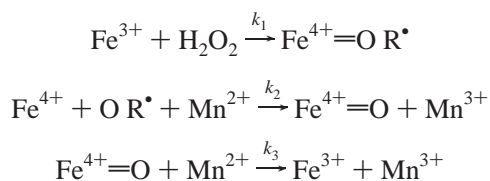
MnP¹ is a member of the ligninase family, which consists of extracellular heme enzymes secreted by the white rot basidiomycetes fungus *Phanerochaete chrysosporium* (*11–14*). These enzymes catalyze the H₂O₂-dependent oxidation of lignin in wood fiber and thus initiate its depolymerization. MnP shares mechanistic features with many other heme peroxidases in which the Fe³⁺ heme reacts with H₂O₂ (*15*) to generate the highly reactive intermediate, Compound I,

consisting of an oxyferryl heme (Fe⁴⁺=O) and a porphyrin π cation radical (*16*). Compound I is then reduced by a one-electron transfer from its reducing substrate to generate Compound II which contains the oxyferryl center but no radical. Compound II finally undergoes further reduction by a second substrate molecule to regenerate the native enzyme (*17*). However, unlike other peroxidases, MnP functions in a rather indirect way, as it appears that lignin is not the direct substrate for the enzyme. Instead, MnP contains a loosely bound Mn²⁺ ion in addition to the heme active site (*11*). The Mn²⁺ is oxidized to the Mn³⁺ state by electron transfer to the hypervalent heme of the oxidized enzyme (Scheme 1), and is believed to dissociate from the enzyme with the aid of dicarboxylic acid chelators such as oxalate (*12, 18–21*) to generate a diffusible oxidant which is believed to be the agent responsible for the degradation of lignin.

¹ Abbreviations: MnP, manganese peroxidase; LiP, lignin peroxidase; CCP, cytochrome *c* peroxidase; CCP(MKT), cytochrome *c* peroxidase produced by expression in *Escherichia coli* containing Met-Lys-Thr at the N-terminus, Ile at position 53, and Gly at position 152; cyt *c*, cytochrome *c*; Compound ES, the H₂O₂ oxidized state of CCP containing the Fe⁴⁺=O heme and Trp-191 cation radical; Compound I, the H₂O₂ oxidized state of most peroxidases containing the Fe⁴⁺=O heme and porphyrin cation radical; Compound II, the one-electron-reduced state of Compound ES or Compound I containing only the Fe⁴⁺=O heme; MPD, 2-methyl-2,4-pentanediol; NMR, nuclear magnetic resonance.

[†] This research was supported by NIH Grant GM48495 to D.B.G., D.E.M., and W.J.C. and Howard Hughes pre-doctoral fellowship to C.D.P.

Scheme 1



The crystal structure of MnP has recently been solved, providing two striking insights (22). First, the overall fold and active site structure of the enzyme are very similar to those of lignin peroxidase (LiP), CCP, and horseradish peroxidase. This includes a histidine as proximal ligand which is strongly hydrogen bonded to an aspartate, and on the distal side, a histidine and arginine that are important for heterolytic peroxy bond cleavage. In addition, MnP contains a bound Mn^{2+} ion, which is directly coordinated to one of the heme propionates. Additional ligands are provided by the carboxylates of Glu-35, Glu-39, and Asp-179, and two coordinated water molecules to provide a roughly octahedral 6-coordinate complex (Figure 1). These findings are gratifying, as it is believed that peroxidases share a common catalytic chemistry at the heme active site, while diversity of function is controlled primarily by how substrates are allowed access to the ferryl heme. In this case, a direct covalent path for efficient electron transfer to the heme center would be established by the heme-coordinated Mn^{2+} . While subsequent mutagenesis studies of the metal ligands of MnP fully support the assignment of this site as the functional Mn^{2+} center (23–25), a number of unresolved questions remain concerning this metal–heme interaction. For example, the role of oxalate as a cofactor has been controversial, and while no oxalate was observed in the crystal structure, it is required for efficient turnover (18, 21, 26). It is possible that the two water ligands may exchange with oxalate to activate the complex or extract and stabilize the Mn^{3+} complex in solution. In addition, it has been proposed that the rate-limiting step in the turnover of MnP is the reduction of Compound II (21, 26–28), but this rate ($\sim 200 \text{ s}^{-1}$) is surprisingly slow for electron transfer of a metal directly coordinated to the heme.

It would thus be of interest to recruit a redox active metal binding site onto the surface of another peroxidase to investigate the potential of such species to undergo intramolecular electron transfer to the ferryl heme center. The goal of this study was to create a functional model for the Mn^{2+} oxidation in manganese peroxidase (MnP) by enlisting the inherent oxidizing potential of another peroxidase. We describe the construction, spectroscopic characterization, and structural properties of manganese binding sites introduced near the heme of cytochrome *c* peroxidase (CCP) by directly wiring the metal to the heme, and show that this metal heme hybrid promotes oxidation of the manganese by the ferryl heme.

MATERIALS AND METHODS

Mutant Construction, Expression, and Purification. The MP6.1–MP6.6 and loop mutants were constructed by oligonucleotide site-directed mutagenesis of single-stranded DNA containing uracil as described previously (29). The MP6.8 mutant was constructed by oligonucleotide site-

directed mutagenesis of double-stranded DNA using the QuikChange Site-Directed Mutagenesis Kit (Stratagene). MP6.1 was used as template upon which Ser at position 181 was reverted to His by cycling 50 ng of template with 125 ng of complementary mutagenic primers for 16 cycles of 12 min each at 68 °C. Expression of CCP(MKT) and these mutants from *E. coli* (30) and purification of these proteins (31) were carried out primarily as described previously. Dialysis of the mutant proteins against distilled water did not result in crystals typically observed during CCP purification. As a result, after the initial purifications, this step was omitted for subsequent purifications. MP6.1 was additionally purified by passage over a Perseptive Biosystems Q/M anion exchange column on a BioCAD Sprint Workstation. The protein was eluted in 50 mM Bis-Tris Propane, 50 mM Tris, pH 6.0, by a salt gradient to 500 mM NaCl. The protein was then dialyzed into 500 mM potassium phosphate buffer, pH 6.0, for storage. MP6.8 was further purified by crystallization by diluting the protein solution 10-fold with 25% 2-methyl-2,4-pentanediol (MPD) on ice after heme reconstitution. The crystal suspension was stored in 25% MPD.

Spectroscopy. UV–vis absorption spectra were collected at 22 °C in 100 mM potassium phosphate, pH 6, and 500 mM potassium phosphate, pH 5, using a Hewlett-Packard 8452A or 8453 diode-array spectrophotometer. Binding assays were performed by difference absorption spectral titrations. Stock solutions of 100 mM MnSO_4 and 100 mM MgSO_4 were prepared in 50 mM sodium tartrate buffer, pH 5.0. Stock protein solutions were diluted into 2.0 mL of 50 mM sodium tartrate buffer, pH 5.0, to give an absorbance of ~ 0.6 at the Soret maximum. The protein was allowed to equilibrate at 22 °C for 30 min in the spectrophotometer with stirring, and the instrument was blanked. An aliquot of the substrate (1 μL of MnSO_4 to MP6.1, MP6.6, and MP6.8; 5 μL of MnSO_4 to WT CCP; 5 μL of MgSO_4 to MP6.1) was added to the cuvette, and the difference absorption spectrum was recorded after 1 min. The dissociation constant for MnSO_4 binding to MP6.1 was determined from a Scatchard plot based on the change at 426 nm. Compound ES was formed by adding 1 equiv of H_2O_2 to approximately 5 μM enzyme in 500 mM potassium phosphate, 1 mM oxalate, pH 5.

Kinetic Measurements. Steady-state kinetics of Mn^{2+} oxidation were measured by incubating enzyme (Soret maximum ~ 0.8) in 50 mM of the appropriate buffer at pH 5.0 (sodium oxalate, sodium lactate, sodium tartrate, or sodium malate). After 15 s, MnSO_4 (0.25–1.0 mM) was added. After an additional 15 s, H_2O_2 (160 μM) was added, and the reaction was observed for 90 s more. K_M and k_{cat} values were calculated from an Eadie–Hofstee plot using the change in absorbance for the formation of the Mn^{3+} –chelator complex (Mn^{3+} –oxalate $\epsilon_{500} = 0.29 \text{ mM}^{-1} \text{ cm}^{-1}$, Mn^{3+} –lactate $\epsilon_{290} = 5.89 \text{ mM}^{-1} \text{ cm}^{-1}$, Mn^{3+} –tartrate $\epsilon_{290} = 2.86 \text{ mM}^{-1} \text{ cm}^{-1}$, and Mn^{3+} –malate $\epsilon_{290} = 4.31 \text{ mM}^{-1} \text{ cm}^{-1}$) (18). Pre-steady-state kinetics of Mn^{2+} oxidation were measured as a function of $[\text{MnSO}_4]$ as follows. The UV–vis absorption spectrum of CCP (WT, MP6.1, and MP6.6) with Soret maximum ~ 0.5 in 500 mM potassium phosphate, 1 mM oxalate, pH 5, was measured. The solution was then mixed with 1 equiv of H_2O_2 and the spectrum measured again to ensure Compound ES formation. MnSO_4 (0.5–5.0 mM) was added and the UV–vis absorption spectrum monitored

until reduction of Compound ES was complete (2 min for MP6.1, MP6.6, and MP6.8, and 30 min for WT). Exponential rates of decay for Compound ES were calculated at 424 nm, and plotted as a function of $[\text{MnSO}_4]$ to determine k_2 and k_3 (Scheme 1).

X-ray Crystallographic Analysis. Single crystals of MP6.8 were grown from 25% MPD by vapor diffusion (32). Crystals were obtained in sitting drops with approximately 0.17 mM MP6.8, 15 mM potassium phosphate, pH 6, 5 mM MnSO_4 , and 10% MPD equilibrated against 25% MPD.² The crystal used to determine the position of the manganese atom in the anomalous difference map was grown from 14 mM potassium acetate, pH 6, 2 mM MnSO_4 . X-ray diffraction data were collected at 100 K using $\text{CuK}\alpha$ radiation from the rotating anode of a Siemens SRA X-ray generator and a Siemens area detector. Data were processed using the Xengen suite of programs (33). Data were analyzed by difference Fourier techniques using XtalView software (34). Models were built using XtalView and refined using repeated cycles of manual adjustment with positional and *B*-factor refinements using the program Shelxl97 (35).

Paramagnetic Nuclear Magnetic Resonance (NMR) Spectroscopy. Wild-type NMR samples were prepared by washing protein crystals 2 times in D_2O , dissolving the crystals in 500 mM potassium phosphate prepared in 99.9% D_2O from Isotec, pH' 6.4 (uncorrected glass electrode meter reading in the deuterated buffer solution), and exchanging the solution twice more with the above buffer. MP6.8 NMR samples were prepared by first chelexing the protein, and then exchanging the buffer 4 times with the deuterated 500 mM potassium phosphate. Enzyme samples (1 mM) were prepared assuming that the molar absorptivity of MP6.8 at the Soret was approximately equal to that for WT-CCP ($\epsilon_{408} = 101.2 \text{ mM}^{-1} \text{ cm}^{-1}$). A 10-fold excess of cyanide was added from a 500 mM KCN solution prepared in deuterated buffer to obtain low-spin ferric enzyme. MnSO_4 was added from a 100 mM stock prepared in D_2O . Spectra were collected for WT CCP, WT CCP plus 3 mM MnSO_4 , MP6.8, MP6.8 plus 0.25 mM MnSO_4 , and MP6.8 plus 1 mM MnSO_4 . Proton NMR experiments were performed on a Bruker AMX 500 spectrometer at 300 K. A total of 5120 scans were acquired for each spectrum, using a spectral width of 31.25 kHz, 8192 complex data points, and a recycle delay of 0.5 s with solvent presaturation. Data were processed in Felix97 (MSI, Inc.). Chemical shift values were referenced to the residual HDO signal at 4.73 ppm.

RESULTS

Cytochrome *c* peroxidase (CCP) was used as a design scaffold for the construction of a functional model of MnP due to its similarity in structure and the ease with which mutant protein can be obtained and structurally characterized. CCP exhibits both sequence (20% amino acid sequence identity) (36) and structural homology to MnP, even though it lacks the Mn^{2+} binding site, Ca^{2+} sites, disulfides, and glycosylation observed in MnP. In the structure of MnP (22),

the manganese is observed to be coordinated by a heme propionate, three carboxylate residues (Glu-35, Glu-39, and Asp-179), and two water molecules (Figure 1A). We have used two approaches to introducing a manganese binding site into CCP: loop transplantation and template-based design. Our first efforts at a model of the manganese binding site in MnP consisted of homology-based transplantation of the metal binding surface loops of MnP onto the structure of CCP. Unfortunately, this approach gave inclusion bodies which could not be reliably reconstituted, suggesting that the alternate conformations of this loop between the two proteins are essential to proper folding of each. These results underscore the potential importance of design into an existing structurally defined matrix.

Design into a Preexisting Scaffold. Several designs for an ersatz MnP were generated by molecular modeling of the existing CCP scaffold, with the goal of introducing one of the heme propionates as a coordinating ligand. The backbone positions in CCP (Gly-41, Val-45, and His-181) that are spatially closest to the Mn^{2+} ligands in MnP (Glu-35, Glu-39, and Asp-179) were identified in the report of the structure of MnP (22). However, comparison of molecular models for the two proteins suggested that using these three positions to contribute metal ligands would be problematic for two reasons. While the C— C_α vectors of Val-45 in CCP and Glu-39 in MnP are similarly directed, this is not true for Gly-41 of CCP and Glu-35 of MnP, because of the additional length and alternate conformation of this loop in CCP (see Figure 1). In addition, the conformation of the CCP loop containing His-181 places it out of range for coordination to the metal site without a significant movement of the main chain. Thus, we have searched for other residue positions in CCP to contribute ligands for a metal coordinated at roughly the same position. One design, MP6.1 (D37E, P44D, V45D, H181S), is shown in Figure 1B as having the same number and type of ligands as MnP, including the heme propionate, three protein-based carboxylates and two water molecules in an octahedral geometry, and bond distances of 2.0–2.1 Å. The additional removal of His-181 was considered to resolve a potential steric clash and to prevent an alternate binding mode with the histidine, as removal of undesired alternate binding modes has been identified as an important design criteria (3). Serine was chosen in an attempt to introduce secondary hydrogen bonding to the Glu-37 ligand. To account for unexpected protein conformational response to mutation and to test for flexibility and variability in the design, additional combinatorial variants of MP6.1 based on the random introduction of either Asp or Glu at positions 37, 44, and 45 were constructed on the H181S background by mutagenesis using a mixed oligonucleotide and verified by DNA sequencing. Initial screening indicated that, in addition to MP6.1, the MP6.6 (D37D, P44D, V45D, H181S) variant exhibited promising behavior, so these two proteins were selected for further study. Initial characterization of these mutant proteins (described below) suggested that His181 might contribute to the structural stability of the protein, so MP6.8 was created from the MP6.1 mutant by reverting residue 181 to His. Fortunately, construction of the closest residue mutant (G41E, V45E, H181D) has been recently reported (1), so that comparisons between these distinctly different designs may be made.

² The crystallographic coordinates for the structure presented in this work have been deposited with the Protein Data Bank, Chemistry Department, Brookhaven National Laboratory, Upton, NY 11973, from which copies are available (entry 1BVA).

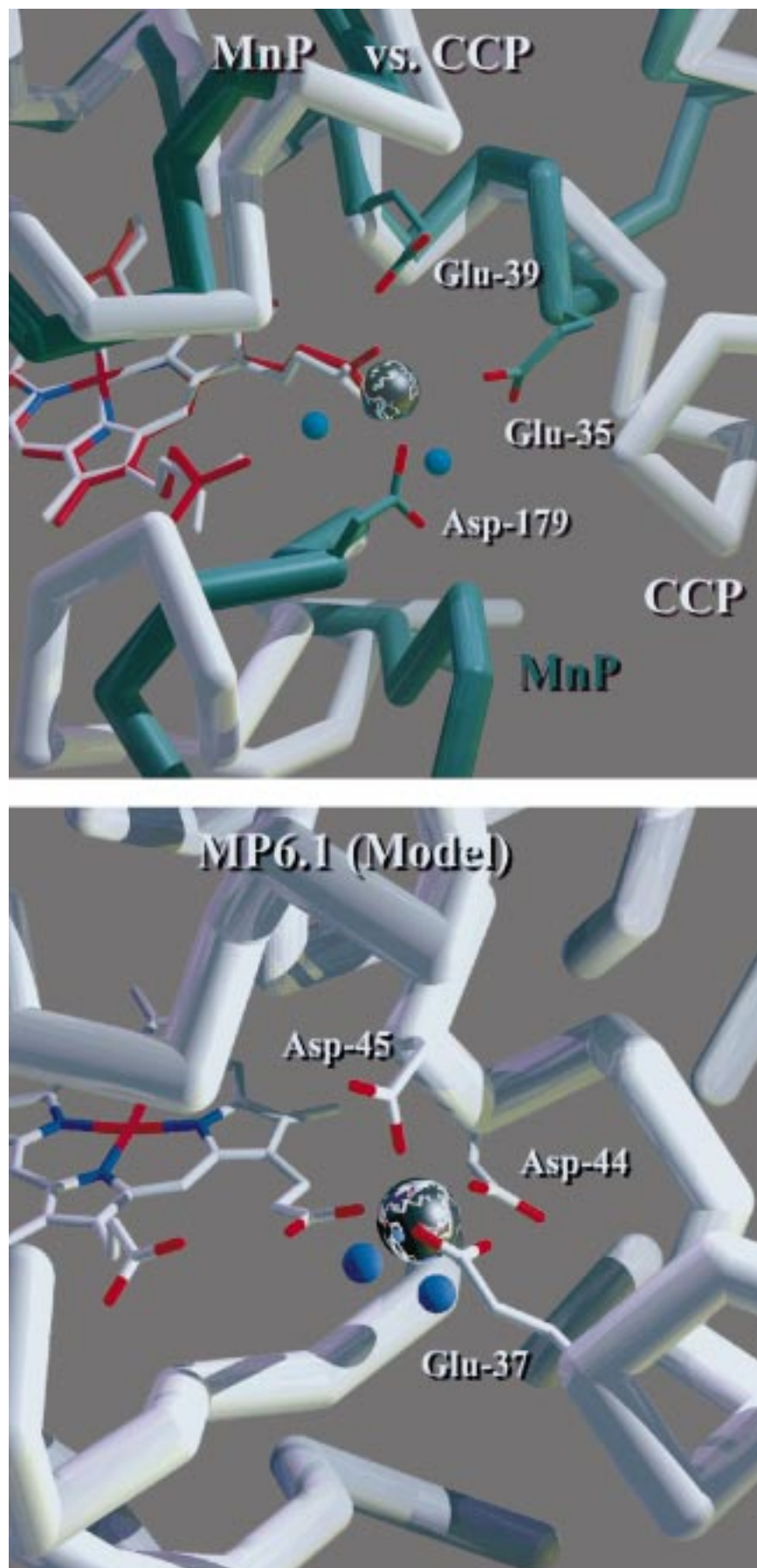


FIGURE 1: Heme environment in MnP and CCP. (A, top) Superposition of the heme groups in MnP (green) and CCP (white). The Mn^{2+} ion and its ligands (two water molecules, heme propionate, E35, E39, and D179) are depicted. (B, bottom) Engineered Mn^{2+} binding site in CCP (MP6.1). The proposed Mn^{2+} is shown bound by two water molecules, a heme propionate, E37, D44, and D45.

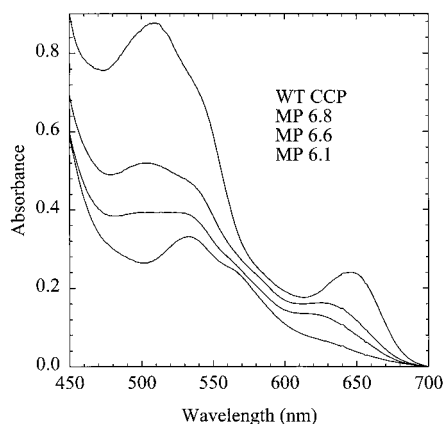


FIGURE 2: Absorption spectra of CCP(MKT), MP6.8, MP6.6, and MP6.1. CCP(MKT) (top), MP6.8 (second), MP6.6 (third), and MP6.1 (bottom) samples were obtained in 500 mM potassium phosphate buffer, pH 5.

Purification of MP6 Mutants. Protein samples for several variants (MP6.1, MP6.6, and MP6.8) were expressed in *E. coli*, purified, and reconstituted with heme using a slightly modified procedure from that used for WT CCP (29, 30). Final dialysis of these mutant proteins did not result in the crystals typically observed at this stage of WT CCP purification. Instead, this step resulted in a precipitate that could not be redissolved in buffer for those variants containing the His181Ser background mutation. For these samples, the crystallization step was omitted, and final purification was accomplished by perfusion ion exchange chromatography. MP6.8 crystals were obtained upon incubation in 25% MPD on ice as a final purification step.

Spectroscopic Properties of the MP6 Variants. The spin states of MP6.1, MP6.6, and MP6.8 were very dependent upon buffer conditions as observed by UV-vis absorption spectra. While WT CCP typically displays high-spin ferric heme in most buffers, MP6 mutant proteins exhibited low-spin UV-vis absorbance spectra in 100 mM potassium phosphate, pH 6.0, with Soret maxima at 412–414 nm and charge transfer bands at 532 and 568 nm. However, at higher salt concentrations and lower pH, such as 500 mM potassium phosphate, pH 5, the MP6 protein family exhibited a variable conversion to the high-spin state ($\lambda_{\text{max}} = 408, 495\text{--}502, 624\text{--}632$ nm). As shown in Figure 2, MP6.1 remained predominantly low-spin, MP6.6 was mixed high- and low-spin, and MP6.8 was predominantly high-spin under these conditions.

Manganese Binding. MP6.1 was observed to bind Mn^{2+} as measured by optical difference titrations. Saturating UV-vis spectroscopic changes in the heme Soret band of MP6.1 were observed upon titration with MnSO_4 in 50 mM sodium tartrate buffer, pH 5.0 (Figure 3). The largest difference feature was a decrease in intensity at 426 nm. A fit to the Scatchard plots of the data gave a Mn^{2+} dissociation constant, $K_d = 175 \mu\text{M}$ for MP6.1. Similar manganese binding properties were observed for MP6.8, the analogous variant containing His-181. However, titration of MP6.6 with Mn^{2+} induced spectroscopic changes which were more complex and did not fit to a simple binding isotherm. Control experiments showed only small nonsaturating changes upon titration of WT CCP with Mn^{2+} . In addition, metal binding by MP6.1 appears to be specific for Mn^{2+} , as control

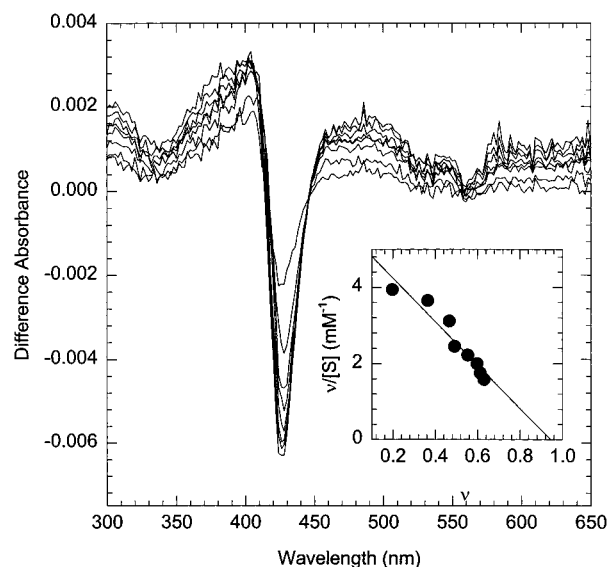


FIGURE 3: Mn^{2+} binding to MP6.1. Optical difference spectra for MP6.1 ($6 \mu\text{M}$) in 50 mM sodium tartrate buffer, pH 5, titrated with successive $1 \mu\text{L}$ additions of 100 mM MnSO_4 at 22 °C. Inset: Scatchard plot utilized to obtain K_d from the difference absorbance at 426 nm, where v is the fraction of enzyme bound with substrate.

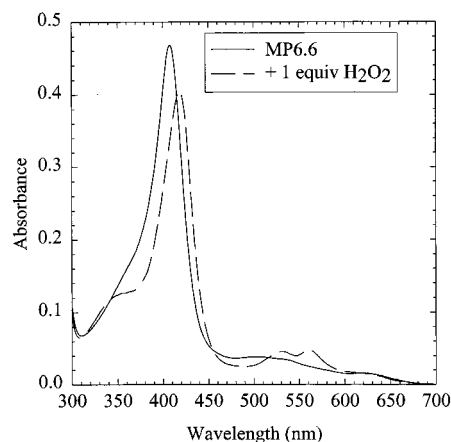


FIGURE 4: Absorption spectra of MP6.6 upon reaction with H_2O_2 . Compound ES (dashed line) was formed by adding 1 equiv of H_2O_2 to $4.6 \mu\text{M}$ MP6.6 in 500 mM potassium phosphate, 1 mM oxalate, pH 5.

titrations with Mg^{2+} also showed only small nonsaturating changes.

Functional Properties. The MP6 mutants were observed to react with H_2O_2 to give a stable oxidized state, and showed enhanced ability to oxidize manganese under steady-state conditions. Under conditions that promote high-spin states of these variants, MP6.1, MP6.6, and MP6.8 react with H_2O_2 to give stable intermediates having UV-vis spectra characterized by a shift of the Soret to 416 nm and α/β bands at 530 and 560 nm (Figure 4), consistent with the formation of an oxyferryl heme center. Under steady-state reaction conditions, the Eadie-Hofstee plots of Figure 5 show that MP6.1, MP6.6, and MP6.8 have significantly enhanced rates of Mn oxidation relative to WT CCP. Kinetic parameters (Table 1) for these reactions show that both k_{cat} and K_M have increased relative to the WT CCP, and that the enhancement in k_{cat} is essentially the same for MP6.1 and MP6.6 and slightly more for MP6.8. While the absolute enzyme turnover rate of these mutants is much less than that of the

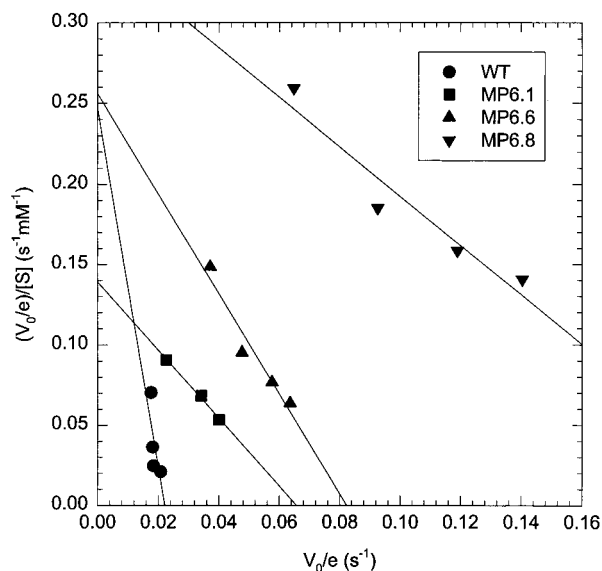


FIGURE 5: Eadie–Hofstee plot for oxidation of Mn^{2+} by wild-type CCP (●), MP6.1 (■), MP6.6 (▲), and MP6.8 (▼). The lines shown are linear least-squares fits to the data. Approximately $8 \mu\text{M}$ enzyme was incubated with $0.25\text{--}1.9 \text{ mM}$ MnSO_4 and $160 \mu\text{M}$ H_2O_2 in 50 mM sodium oxalate, pH 5, at 22°C . The formation of Mn^{3+} –oxalate was measured at 500 nm ($\epsilon = 0.29 \text{ mM}^{-1} \text{ cm}^{-1}$) (18).

Table 1: Steady-State Manganese Peroxidase Activities

enzyme	k_{cat} (s^{-1})	K_M (mM)	k_{cat}/K_M ($\text{mM}^{-1} \text{ s}^{-1}$)
WT	0.0265	0.102	0.260
MP6.1	0.118	0.574	0.205
MP6.6	0.122	0.369	0.331
MP6.8	0.216	0.654	0.330
MnP ^a	301	0.0694	4340

^a MnP values from Mayfield et al. (1994) were in 50 mM sodium malonate, pH 4.5, with $0.5 \mu\text{g/mL}$ MnP, 0.1 mM H_2O_2 , and $0.025\text{--}0.5 \text{ mM}$ MnSO_4 (40).

native MnP enzyme ($\sim 0.1\%$) (18, 20, 26), the introduced activity is significant. Control experiments show that this increase in Mn oxidation activity is not a result of a general increase in reactivity of the mutants, as aniline oxidation by MP6.6 was essentially identical to that of WT CCP (data not shown). Finally, as shown in Figure 6, this activity was stimulated by and displays a dramatic sensitivity to dicarboxylic acid chelators present in the reaction medium.

Kinetics of Electron Transfer from Mn^{2+} to Ferryl Heme. The rate constants for the reaction of Compound ES with Mn^{2+} (k_2) and for the reaction of Compound II with Mn^{2+} (k_3) (see Scheme 1) were measured. These rates are of interest as it is likely that the differences in rates reflect the difference in electron transfer from the Mn^{2+} to the Trp-191 radical of Compound ES (k_2) and to the ferryl heme of Compound II (k_3). Compound ES was generated by reaction of the enzyme with 1 equiv of H_2O_2 immediately before rapid mixing with an excess of Mn^{2+} . The decay of the oxyferryl heme was monitored at 424 nm . Over the same time scale, the decay of the ferryl state in the absence of Mn^{2+} for each protein was negligible. The observed decay was biphasic with an initial lag as shown in Figure 7. This lag phase has been well characterized for CCP reactions and is due to the fact that the initial reaction with Compound ES reduces the Trp-191 radical, and thus contributes nothing to the change in the ferryl heme absorbance (37). The kinetics for the

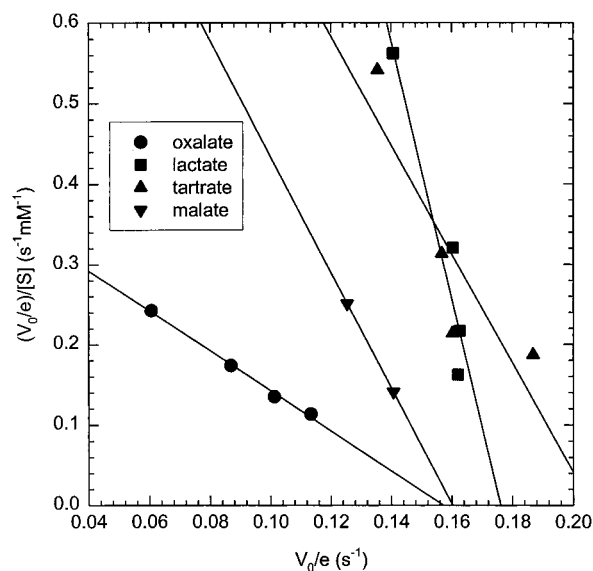


FIGURE 6: Effect of chelator identity on Mn^{2+} oxidation by MP6.6. Eadie–Hofstee plots are shown for the oxidation of MnSO_4 in the presence of various chelators. The lines shown are linear least-squares fits to the data. Approximately $8 \mu\text{M}$ enzyme was incubated with $0.25\text{--}1.0 \text{ mM}$ MnSO_4 and $160 \mu\text{M}$ H_2O_2 in 50 mM buffer, pH 5, at 23°C . The formation of Mn^{3+} complex was monitored (Mn^{3+} –oxalate $\epsilon_{500} = 0.29 \text{ mM}^{-1} \text{ cm}^{-1}$, Mn^{3+} –lactate $\epsilon_{290} = 5.89 \text{ mM}^{-1} \text{ cm}^{-1}$, Mn^{3+} –tartrate $\epsilon_{290} = 2.86 \text{ mM}^{-1} \text{ cm}^{-1}$, and Mn^{3+} –malate $\epsilon_{290} = 4.31 \text{ mM}^{-1} \text{ cm}^{-1}$) (18).

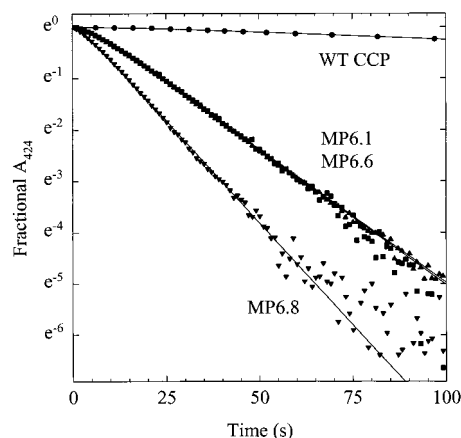


FIGURE 7: Pre-steady-state oxidation of Mn^{2+} by wild-type CCP (●), MP6.1 (■), MP6.6 (▲), and MP6.8 (▼). Approximately $5 \mu\text{M}$ enzyme in 500 mM potassium phosphate, 1 mM oxalate, pH 5, was mixed with 1 equiv of H_2O_2 to form Compound ES. MnSO_4 (2.5 mM) was added and the UV–vis absorption spectrum monitored until reduction of Compound ES was complete (2 min for MP6.1 and MP6.6 and 30 min for WT). Exponential rates of decay for Compound ES were calculated at 424 nm and fit to eq 1.

Table 2: Pre-Steady-State Rates of Electron Transfer from Mn^{2+} to CCP Compound I

protein	k_2^{obs} (s^{-1})	% WT	k_3^{obs} (s^{-1})	% WT
WT	0.065	100	0.0029	100
MP6.1	0.232	356	0.058	1817
MP6.6	0.268	412	0.052	1788
MP6.8	0.530	821	0.080	2741

decay of the oxyferryl heme moiety are thus expected to follow eq 1. As shown in Figure 7, the data fit well to this mechanism to give the parameters shown in Table 2, indicating that electron transfer from Mn^{2+} both to the Trp-191 radical and to the ferryl heme is faster for the MP6

Table 3: X-ray Diffraction Data Collection and Refinement Statistics^a

Data Collection	
unit cell	
<i>a</i> (Å)	105.8
<i>b</i> (Å)	73.6
<i>c</i> (Å)	50.5
resolution (Å)	1.88
<i>I</i> / σ_1 (av)	18.8
<i>I</i> / σ_1 (last shell)	2.4
no. of reflections	26232
completeness (%)	81
<i>R</i> _{sym}	5.2
Refinement	
<i>R</i> _{cryst}	0.179
resolution (Å)	1.88
no. of reflections	25534
rms _{bond} (Å)	0.006
rms _{angle} (deg)	1.7
no. of waters	363

^a Data were collected at 100 K on a Siemens 3 axis area detector using Cu K α radiation and processed using the Xengen suite of programs (33). The model was built using the XtalView software (34) and refined in Shelxl97 (35). The data set was collected on a single crystal, and *R*_{sym} represents the agreement between *F*_o for equivalent reflections. Values of *I*/ σ_1 (last shell) represent the average *I*/ σ_1 for the 10% of the data of highest resolution. The *R*_{cryst} value is the crystallographic residuals for the observed and model-derived structure factor amplitudes for all data.

variants than for WT CCP. Additionally, these rates were observed to be dependent on [MnSO₄], yielding bimolecular rate constants of 0.0140 and 0.00104 mM⁻¹ s⁻¹ for WT *k*₂ and *k*₃, respectively, 0.0724 and 0.0152 mM⁻¹ s⁻¹ for MP6.6 *k*₂ and *k*₃, respectively, and 0.0698 and 0.0142 mM⁻¹ s⁻¹ for MP6.8 *k*₂ and *k*₃, respectively.

$$\frac{A'_{424} - A_{424}^{t=\infty}}{A_{424}^{t=0} - A_{424}^{t=\infty}} = \frac{1}{k_3^{\text{obs}} - k_2^{\text{obs}}} (k_3^{\text{obs}} e^{-k_2^{\text{obs}} t} - k_2^{\text{obs}} e^{-k_3^{\text{obs}} t}) \quad (1)$$

Structural Studies. A low-temperature crystal structure of MP6.8 reveals both similarities and differences with the designed metal binding site. Crystallization trials were performed for each of the purified MP6 variants, but MP6.1 and MP6.6 could not be crystallized under variations of conditions known to be effective for WT CCP and most mutants. However, for MP6.8, high-quality crystals could be obtained in the presence or absence of 5 mM MnSO₄. A low-temperature diffraction data set for MP6.8/Mn was collected at 100 K that was 87% complete to 1.9 Å (Table 3). A model was fit to the initial electron density and refined to 1.9 Å resolution (final *R* = 17.9%). The structure, when compared with that of WT CCP, showed (Figure 8) that the overall structures were very similar, but that the loop from Asp-34 to Tyr-42 had undergone a conformation change. Due to contact with this loop, a smaller shift in the backbone of residues Ala-193 to Asn-196 occurred. The main chain for two of the proposed Mn²⁺ ligands, Asp-44 and Asp-45, was observed in the designed conformation, as was the side chain of Asp-45. The side chain of Asp-44 was pointing away from the designed metal site, as a steric clash with the new position of the residue 34–42 loop would prevent its position as designed. The side chain of Glu-37 was significantly displaced from its designed position due to its presence on the 34–42 loop, and appeared disordered as its density was

not evident beyond C α . An electron density peak was observed between the heme propionate and the Asp-45 carboxylate at distances of 2.3 and 2.8 Å, respectively. While these distances are somewhat longer than expected from inorganic Mn²⁺ complexes, it is noted that the distances observed between the Mn²⁺ and its ligands in native MnP ranged from 2.32 Å for the propionate to 2.82 Å for Glu-39, the analogous residue to Asp-45. Thus, the metal to ligand distances observed for the MP6.8 model are nearly identical with those of the corresponding ligands in MnP. When refined as a water molecule, this peak gave a *B* value of 24, indicating that it is either a well-ordered water or a weakly occupied metal. Additional experiments confirmed the assignment of the electron density to manganese ion binding. First, an X-ray data set collected on an MP6.8 crystal grown in the absence of Mn²⁺ showed similar rearrangements in the loop residues noted above, but gave no evidence of electron density at the position of the putative metal ion. An additional X-ray data set collected on a crystal of MP6.8 grown in 2 mM MnSO₄ in acetate buffer was used to construct an anomalous scattering difference map. The effective concentration of Mn²⁺ is higher in this structure since manganese acetate is more soluble than manganese phosphate. This map, shown in Figure 9, shows two strong features at the position of the heme iron and the metal ion binding site. These peaks can only arise from centers which contribute anomalous scattering intensity to give rise to differences in intensities for Bijvoet pairs of reflections. The presence of an anomalous scattering peak at the metal ion site shows conclusively that the site is occupied by a metal ion and not water.

Finally, one-dimensional NMR spectra of MP6.8 show that the presence of Mn²⁺ causes notable paramagnetic broadening of two proton resonances in the upfield region of the spectrum (Figure 10). Recently Yeung et al. reported a similar observation and assigned it to paramagnetic broadening of the 7-propionate β protons due to rapid spin relaxation by the divalent cation Mn²⁺. These resonances in WT-CCP were unaffected by addition of a 3-fold excess of Mn²⁺. The above observation, taken in conjunction with the previously reported results (1, 38) and our X-ray crystallographic structure of MP6.8, indicates that Mn²⁺ is interacting with the heme 7-propionate ligand as designed.

DISCUSSION

The spectroscopic, functional, and structural properties of the MP6 designs, when compared to those of native MnP, traditional peroxidases, and a previously reported model for a similar site in CCP, provide an interesting picture of what is important and necessary for the oxidation of Mn²⁺ in a heme peroxidase. These properties further provide valuable information for future metalloprotein design efforts. Primarily, the fact that several variant designs have shown stimulated MnP activity in CCP demonstrates the validity of the approach of engineering function into this enzyme and supports the hypothesis that providing substrate access to the oxidized heme center is an effective first-priority design criteria. The details of the functional and structural differences between our models and MnP provide important information about the functional requirements for Mn²⁺ oxidation. Differences between our models and the intended

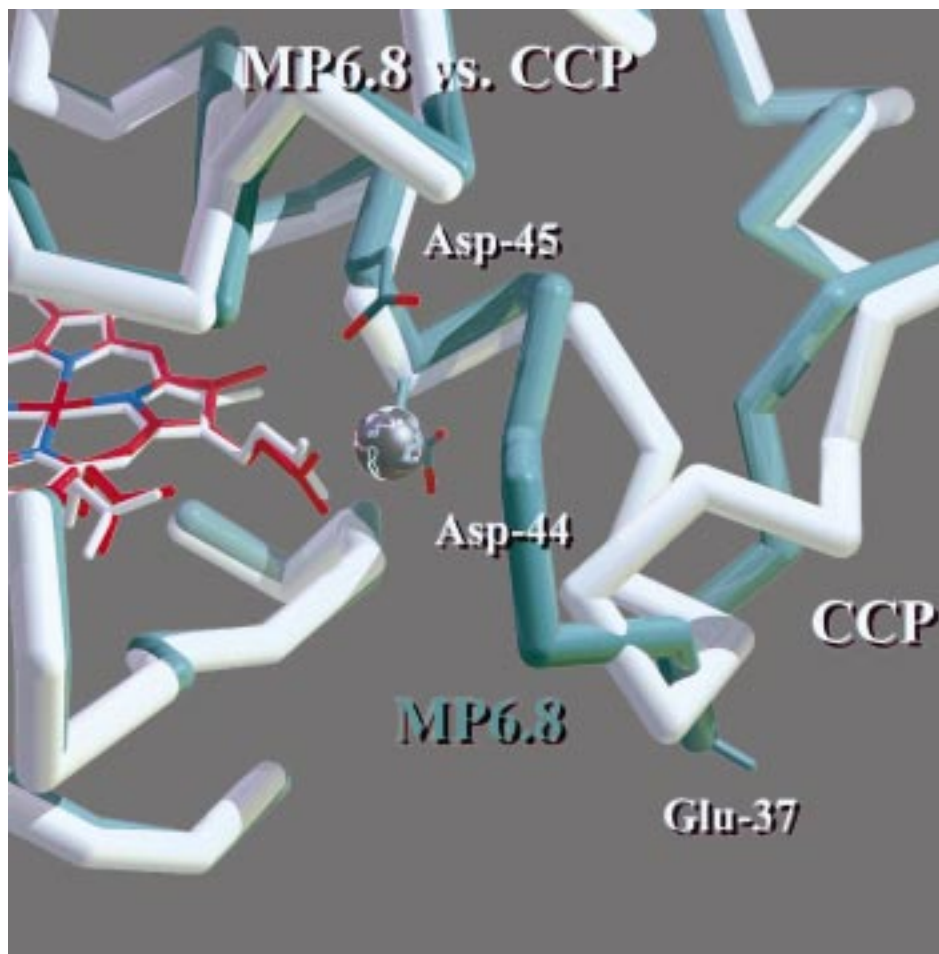


FIGURE 8: Comparison of the backbone for refined models of wild-type CCP and MP6.8. The wild-type CCP structure (white) is overlaid on that of MP6.8 (green), grown in the presence of 5 mM MnSO_4 in phosphate. The position of the electron density for the partially occupied metal is represented by the metallic sphere.

design show how these models may be improved in the future.

The properties of the MP6 designs provide insight into the function of native MnP. The Mn^{2+} affinity for MP6.1 (175 μM) is only 4-fold weaker than that observed for native MnP under the same conditions ($K_d = 46 \mu\text{M}$) (18), and is very similar to that reported for the G41E, V45E, H181D “closest residue” triple mutant of CCP ($K_d = 125 \mu\text{M}$) (1). As a reversibly bound substrate, it is important that Mn^{2+} not bind too tightly to the enzyme, and it is evident that it is not difficult to introduce artificial binding affinity of this magnitude. The binding of Mn^{2+} caused a similar type of broadening in the ^1H NMR spectrum of MP6.8 as was observed for the “closest residue” triple mutant and attributed to the paramagnetic broadening of the 7-propionate β protons due to rapid spin relaxation by the divalent cation Mn^{2+} [Yeung et al. (1997) (1)]. We note that, in addition to similar Mn^{2+} binding, Yeung et al. also report similar enhanced rates of MnP activity by the “closest residue” triple mutant (1). Again, this intriguing result indicates that there is more than one way in which a functional binding site for manganese oxidation can be installed near the heme periphery.

Native MnP is known to require cofactors such as oxalate for efficient manganese oxidation, and these agents appear to affect the values of K_M more than those of k_{cat} (20, 26). This is consistent with proposals that these cofactors function as chelators to extract and stabilize the Mn^{3+} product from

the enzyme site. It is quite significant that for the reactions of MP6.6 in Figure 6, the most significant effect of the type of dicarboxylic acid used is on the slope, from which the apparent K_M values are determined. This trend indicates that the role of such cofactors may be a general property of these sites defined by the need for efficient extraction of the oxidized Mn^{3+} product. Additionally, several conclusions regarding the details of electron-transfer reactions between the designed Mn^{2+} site and the oxidized heme center can be drawn from these studies. The spectroscopically “silent” rate constant (k_2^{obs}), which corresponds to reduction of the Trp-191 radical of CCP compound ES, is significantly faster than that for reduction of the ferryl heme for all four enzyme variants. As has been noted, this may be due to an efficient intramolecular electron redistribution between ferryl and Trp radical, and does not necessarily indicate that the initial reduction is proceeding directly into the Trp-191 residue. For example, the ferryl may be directly reduced, but rapidly reoxidized by the Trp radical to give the appearance that Mn^{2+} is reacting first with the Trp (39). Each of the MP6 variants undergoes both electron-transfer reactions with Mn^{2+} more rapidly than does WT CCP. Finally, the introduction of the manganese binding site causes a greater effect on the rate of ferryl reduction (k_3^{obs}) than on the initial rate of disappearance of the Trp radical (k_2^{obs}). This suggests that the mutations have directly assisted the ability of Mn^{2+} to donate electrons into the ferryl heme. The fact that both

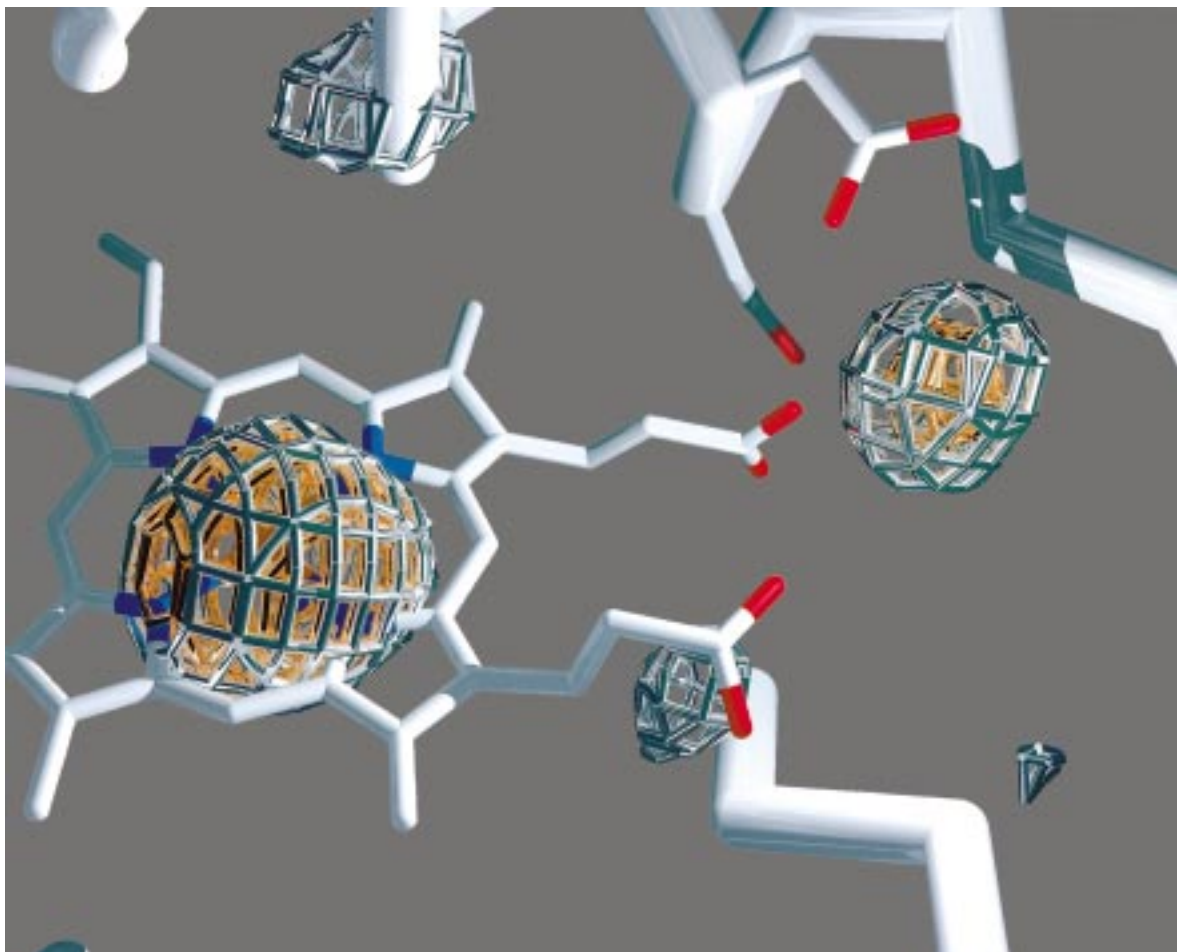


FIGURE 9: Anomalous scattering in the X-ray crystal structure of MP6.8 grown in the presence of MnSO_4 . $|F_o| - |F_c|$ electron density map, contoured at 3 and 4σ , is superimposed upon the refined model of and MP6.8 crystal grown in 2 mM MnSO_4 in acetate.

reactions are slow, given the direct coupling of the proposed binding site to the heme, is not inconsistent with known properties of both CCP and MnP. The Compound ES state of MP6 mutants is expected to differ from Compound I of MnP in that the former contains a ferryl heme and Trp-191 radical, while it is believed that the latter contains the radical directly on the porphyrin. Electron transfer from Mn^{2+} to Compound I of MnP is much faster than to Compound II. Likewise, it is not surprising that both reactions are slow for MP6, because neither contains radical species on the porphyrin.

The properties of the MP6 mutants also provide insight into the process of metal site design. The tendency of all mutants to revert to the high-spin configuration under high-salt and/or low-pH conditions may be the result of negating the effects of the several charged carboxylates that have been introduced in close proximity. Thus, either high ionic strength to promote electrostatic screening and ion-pair interactions or lower pH to protonate one or more of the carboxylates would be expected to have the same stabilizing effect. The fact that MP6.8 (retaining His-181) is more easily converted to the active high-spin state and is more readily crystallized than MP6.1 (containing Ser-181) indicates that His-181 is important for the structural integrity of the protein. His-181 was removed in the design of MP6.1 to prevent possible unfavorable steric interactions with Glu-37 and to prevent possible competition by His-181 for metal binding. Our results indicate that negative design, while clearly an

important consideration, may often present its own structural problems. The close proximity of the His-181 side chain to the designed position of Glu-37 may be the source of the conformational change observed in the loop between residues 34 and 42, which repositions Glu-37 away from the site.

It is also interesting to compare the properties of the MP6 designs with the closest residue model reported earlier (1). It was not clear to us that residues 41, 45, and 181 could be utilized to generate a similar metal site in CCP. For example, the surface loops on MnP containing Asp-179 and Glu-35 are in a significantly different conformation and are different lengths in the two enzymes (Figure 1). The closest residue in CCP to Asp-179 is His-181, which is moved far enough away in CCP that no residue at this position would coordinate to the native metal site without significant changes in the protein. In addition, Glu-35 in MnP extends toward the N-terminal side of α -helix B, while in CCP this helix is truncated by about one turn so that the equivalent residue, Gly-41, is pointing away from the metal. Again, simple introduction of a carboxylate at position 41 would necessitate a significant change in backbone structure to bind metal. Thus, the similar Mn^{2+} binding and functional properties of these two designs were unexpected until examination of the structure of MP6.8. The two designs have a carboxylate group at position 45 and the heme propionate in common. However, the rearrangement observed for MP6.8 in the 34–42 loop, which removes Glu-37 from a coordinating conformation, probably results in the same effect as attempting

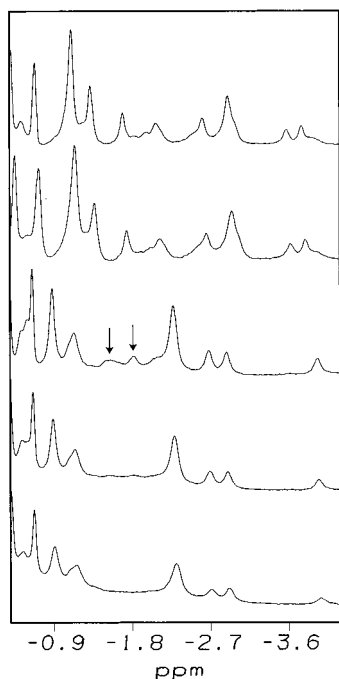


FIGURE 10: Effect of Mn^{2+} on the paramagnetic 1H NMR spectra of CCP(MKT) and MP6.8. The upfield spectra of CCP(MKT) (top), CCP(MKT) plus 3 mM $MnSO_4$ (second), MP6.8 (third), MP6.8 plus 0.25 mM $MnSO_4$ (fourth), and MP6.8 plus 1 mM $MnSO_4$ (bottom) are shown. 500 MHz spectra of 1 mM enzyme were collected at 300 K in deuterated 500 mM potassium phosphate, pH 6.4. Arrows indicate the resonances in MP6.8 attributed to the 7-propionate β protons.

to utilize residue 35 for that purpose. These results suggest that utilizing Glu-84 instead of residues in the 34–42 loop will be much more effective in improving future designs.

ACKNOWLEDGMENT

We thank Dr. Z. Hu for mutagenesis of MP6 and Dr. M. Gold for graciously providing a sample of MnP. We also thank Dr. G. M. Jensen, Dr. A. Khindaria, Dr. J. T. Murphy, Dr. R. A. Musah, R. J. Rosenfeld, and Dr. P. A. Williams for helpful discussions and critical comments.

REFERENCES

- Yeung, B. K. S., Wang, X., Sigman, J. A., Petillo, P. A., and Lu, Y. (1997) *Chem. Biol.* 4, 215–221.
- Hellinga, H. W. (1996) *Curr. Opin. Biotechnol.* 7, 437–441.
- Hellinga, H. W. (1996) in *Protein Engineering: Principles and Practice* (Cleland, J. L., and Craik, C. S., Eds.) pp 369–398, Wiley-Liss Inc., New York.
- Suh, S. S., Haymore, B. L., and Arnold, F. H. (1991) *Protein Eng.* 4, 301.
- Higaki, J. N., Haymore, B. L., Chen, S., Fletterick, R. J., and Craik, C. S. (1990) *Biochemistry* 29, 8582–8586.
- Roberts, V. A., Iverson, B. L., Iverson, S. A., Benkovic, S. J., Lerner, R. A., Getzoff, E. D., and Tainer, J. A. (1990) *Proc. Natl. Acad. Sci. U.S.A.* 87, 6654–6658.
- Stewart, J. D., Roberts, V. A., Crowder, M. W., Getzoff, E. D., and Benkovic, S. J. (1994) *J. Am. Chem. Soc.* 116, 415–416.
- Coldren, C. D., Hellinga, H. W., and Caradonna, J. P. (1997) *Proc. Natl. Acad. Sci. U.S.A.* 94, 6635–6640.
- Bonagura, C. A., Sundaramoorthy, M., Pappa, H. S., Patterson, W. R., and Poulos, T. L. (1996) *Biochemistry* 35, 6107–6115.
- Pinto, A. L., Hellinga, H. W., and Caradonna, J. P. (1997) *Proc. Natl. Acad. Sci. U.S.A.* 94, 5562–5567.
- Tien, M., and Kirk, T. K. (1983) *Science* 221, 661–663.
- Glenn, J. K., and Gold, M. H. (1985) *Arch. Biochem. Biophys.* 242, 329–341.
- Pease, E. A., Aust, S. D., and Tien, M. (1991) *Biochem. Biophys. Res. Commun.* 179, 897–903.
- Mayfield, M. B., Godfrey, B. J., and Gold, M. H. (1994) *Gene* 142, 231–235.
- Yonetani, T. (1976) in *Enzymes* (Boyer, P. D., Ed.) pp 345–61, Academic Press, New York.
- Dolphin, D., Forman, A., Borg, D. C., Fajer, J., and Felton, R. H. (1971) *Proc. Natl. Acad. Sci. U.S.A.* 68, 614–618.
- Coulson, A. F. W., Erman, J. E., and Yonetani, T. (1971) *J. Biol. Chem.* 246, 917–924.
- Wariishi, H., Valli, K., and Gold, M. H. (1992) *J. Biol. Chem.* 267, 23688–23695.
- Aitken, M. D., and Irvine, R. L. (1990) *Arch. Biochem. Biophys.* 276, 405–414.
- Kuan, I. C., Johnson, K. A., and Tien, M. (1993) *J. Biol. Chem.* 268, 20064–20070.
- Kuan, I. C., and Tien, M. (1993) *Proc. Natl. Acad. Sci. U.S.A.* 90, 1242–1246.
- Sundaramoorthy, M., Kishi, K., Gold, M. H., and Poulos, T. L. (1994) *J. Biol. Chem.* 269, 32759–32767.
- Kishi, K., Hildebrand, D. P., Kusters-van Someren, M., Gettemy, J., Mauk, A. G., and Gold, M. H. (1997) *Biochemistry* 36, 4268–4277.
- Kishi, K., Kusters-van Someren, M., Mayfield, M. B., Sun, J., Loehr, T. M., and Gold, M. H. (1996) *Biochemistry* 35, 8986–8994.
- Whitwam, R. E., Brown, K. R., Musick, M., Natean, M. J., and Tien, M. (1997) *Biochemistry* 36, 9766–9773.
- Kishi, K., Wariishi, H., Marquez, L., Dunford, H. B., and Gold, M. H. (1994) *Biochemistry* 33, 8694–8701.
- Wariishi, H., and Gold, M. H. (1990) *J. Biol. Chem.* 265, 2070–2077.
- Wariishi, H., Marquez, L., Dunford, H. B., and Gold, M. H. (1990) *J. Biol. Chem.* 265, 11137–11142.
- Goodin, D. B., and McRee, D. E. (1993) *Biochemistry* 32, 3313–3324.
- Fitzgerald, M. M., Churchill, M. J., McRee, D. E., and Goodin, D. B. (1994) *Biochemistry* 33, 3807–3818.
- Goodin, D. B., Davidson, M. G., Roe, J. A., Mauk, A. G., and Smith, M. (1991) *Biochemistry* 30, 4953–4962.
- Wang, J. M., Mauro, J. M., Edwards, S. L., Oatley, S. J., Fishel, L. A., Ashford, V. A., Xuong, N. H., and Kraut, J. (1990) *Biochemistry* 29, 7160–7173.
- Howard, A. J., Nielson, C., and Xuong, N. H. (1985) in *Methods in Enzymology* (Wyckoff, H. W., Hirs, C. H. W., and Timasheff, S. N., Eds.) pp 452–472, Academic Press, Inc., Orlando, FL.
- McRee, D. E. (1992) *J. Mol. Graphics* 10, 44–46.
- Sheldrick, G. M. (1997) in *Methods in Enzymology* (Carter, C. W. Jr., and Sweet, R. M., Eds.), Academic Press, New York.
- Welinder, K. G. (1992) *Curr. Opin. Struct. Biol.* 2, 388–393.
- Roe, J. A., and Goodin, D. B. (1993) *J. Biol. Chem.* 268, 20037–20045.
- Satterlee, J. D., Erman, J. E., Mauro, J. M., and Kraut, J. (1990) *Biochemistry* 29, 8797–8804.
- Millett, F., Miller, M. A., Geren, L., and Durham, B. (1995) *J. Bioenerg. Biomembr.* 27, 341–351.
- Mayfield, M. B., Kishi, K., Alic, M., and Gold, M. H. (1994) *Appl. Environ. Microbiol.* 60, 4303–4309.

BI9815039